ACS APPLIED MATERIALS & INTERFACES

Research Article

Cite This: ACS Appl. Mater. Interfaces 2018, 10, 16458−16466

www.acsami.org

Synergistic Effect between $LiNi_{0.5}Co_{0.2}Mn_{0.3}O_2$ and $LiFe_{0.15}Mn_{0.85}PO_4$/C on Rate and Thermal Performance for Lithium Ion Batteries

Guiyan Sun, Shaobo Lai, Xiangbang Kong, Zhiqiang Chen, Kun Li, Rong Zhou, Jing Wang,* and Jinbao Zhao*

State Key Laboratory of Physical Chemistry of Solid Surfaces, Collaborative Innovation Center of Chemistry for Energy Materials, State-Province Joint Engineering Laboratory of Power Source Technology for New Energy Vehicle, College of Chemistry and Chemical Engineering, Xiamen University, Xiamen 361005, China

Supporting Information

ABSTRACT: A blend cathode has been prepared by mixing both $LiNi_{0.5}Co_{0.2}Mn_{0.3}O_2$ (NCM523) of high energy density and high specific capacity and $LiFe_{0.15}Mn_{0.85}PO_4$/C (LFMP/C) of excellent thermal stability via a low-speed ball-milling method. The lithium ion batteries using the blend cathode with LFMP/C of optimum percent exhibit better capacity retention after 100 cycles than those using only single NCM523 or LFMP/C. Both theoretical simulation and experimental rate performances demonstrate that the electrochemical property of blend cathode materials is predictable and economical. In addition, the thermal behaviors of blend cathodes are studied by using differential scanning calorimetry analysis. The thermal stability of blend cathode materials behaves better than that of the bare NCM523 accompanied with an electrolyte. It is found that the outstanding rate and thermal performance of the blend cathode is due to the prominent synergistic effect between NCM523 and LFMP/C, and 10% LFMP/C in the blend cathode materials is the most adaptable as considering both electrochemical and thermal properties simultaneously.

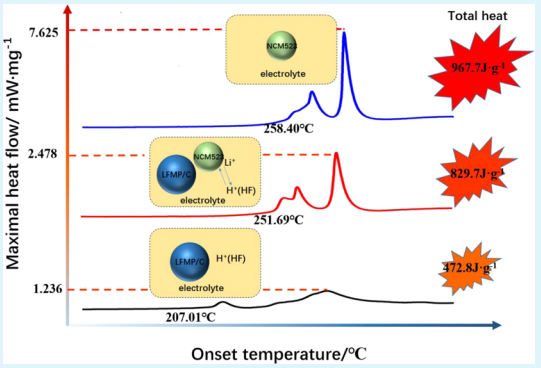

KEYWORDS: *$LiNi_{0.5}Co_{0.2}Mn_{0.3}O_2$, $LiFe_{0.15}Mn_{0.85}PO_4$/C, blend cathode, thermal stability, lithium ion battery*

1. INTRODUCTION

Lithium ion batteries (LIBs) have been significantly applied in 3C electronic equipment, electrical vehicles, and plug-in hybrid electric vehicles (PHEVs) as secondary batteries because of their high energy density, long cycle life, and almost no memory effects.[1−4] Although researchers have made lots of efforts to develop more wide application of LIBs, the thermal safety problem, especially when they are in abuse, is one of the critical problems that block their further application.[5−7]

According to lots of previous works, the cathode dominates the actual capacity of the whole battery, which provides the active lithium in the battery. The capacity contribution of anode materials is always redundant over cathode materials, no matter the commercialized graphite (372 mA h/g) or promising silicon (4200 mA h/g).[8−10] Among various kinds of cathode materials, $LiNi_xCo_yMn_zO_2$ (NCM, $x + y + z = 1$) is drawing more and more attention for its excellent specific capacity and energy density. With a typical α-$NaFeO_2$ layered structure, the NCM possesses favorable behaviors of $LiNiO_2$, $LiCoO_2$, and $LiMnO_2$ at the same time associating with the high capacity of nickel (Ni), excellent rate capability of cobalt (Co), and outstanding safety of manganese (Mn).[11,12]

Among the main parts in LIBs, the cathode predominately dominates the thermal behaviors when the thermal runaway happens. Therefore, lots of research studies have been done to improve the thermal stability of the cathode. Doping metal ions into the crystal structure of NCM,[13−15] coating the NCM with more stable materials,[16−18] and blending the NCM with other cathodes[19−21] are generally adopted methods to improve the thermal stability of the NCM cathode. Blending the NCM with olivine cathodes may be in consideration of economic efficiency, complex degree, and so on. As reported in previous research studies,[16,21] the olivine could be a suitable component to blend with layered oxide because of its low cost, environmental friendliness, high thermal stability, and other excellent electrochemical properties. Because of the addition of a more stable cathode material, the blending cathodes will attract more application in HEVs and the PHEVs.

As one kind of typical olivine, $LiFe_xMn_yPO_4$ (LFMP, $x + y = 1$) possesses a *pnma* space group, which is identical to $LiFePO_4$ (LFP) and $LiMnPO_4$ (LMP). Furthermore, the LFMP exhibits higher average potential and energy density than the LFP and a better conductivity than the LMP.[22,23] Both polyanion $(PO_4)^{3-}$ and covalent bond P−O will make the LFMP have a stable framework and an excellent thermally stable cathode material compared to other phosphates.[24]

Received: February 4, 2018
Accepted: April 24, 2018
Published: April 24, 2018

DOI: 10.1021/acsami.8b02102
ACS Appl. Mater. Interfaces 2018, 10, 16458−16466

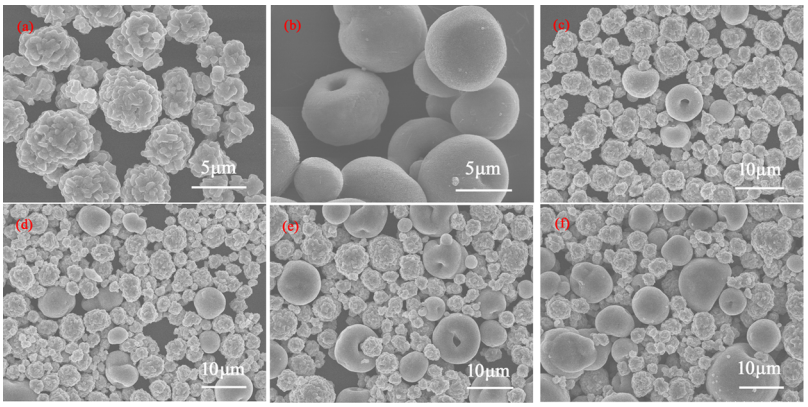

Figure 1. SEM images of (a) NCM523, (b) LFMP/C, (c–f) 5% blend, 10% blend, 20% blend, and 30% blend materials.

It is well-known that the crystal structure of electrode materials changes greatly during charge and discharge processes. When charged to 4.3 V, the crystal structure of delithiated NCM differs from that of lithiated NCM. Ni^{4+} in NCM tends to convert to more stable Ni^{2+} along with O_2 release during delithiation process with the temperature rising, which is often followed by a reaction between the NCM and the electrolyte. Then, the highly delithiated NCM may lead to a thermal runaway of the whole battery because of the heat released from the reaction between O_2 and organic solvent.[25,26] Hence, it is significant to improve the thermal stability of the cathode material.

In this work, the blend cathode materials are prepared by mixing NCM523 with the LFMP/C material through a ball-milling method without damage of the microstructure and crystal structure. The electrochemical and thermal characters have suggested that the blend materials exhibit not only excellent electrochemical property offered by NCM523 but also high thermostability provided by LFMP/C. The blend cathode materials can combine the advantages of both LFMP/C and NCM523 together. In addition, there is an obvious synergistic effect of thermal behavior between LFMP/C and NCM523, which was verified by differential scanning calorimetry (DSC) and X-ray diffraction (XRD) testing.

2. EXPERIMENTAL SECTION

2.1. Materials and Cell Preparation. The commercial $LiNi_{0.5}Co_{0.2}Mn_{0.3}O_2$ (NCM523, ~4.3 μm, Beijing Easpring Materials Technology Co., Ltd) and $LiFe_{0.15}Mn_{0.85}PO_4$/C (LFMP/C, ~9.8 μm, China Aviation Lithium Battery Co., Ltd) were used to prepare the blend cathode materials. The blend materials were prepared by mixing NCM523 with LFMP/C in a ball-milling instrument (FRITSCH, Germany) with moderate milling balls and obtained after gentle milling for 15 min with a speed of 100 rpm, which are marked with the weight ratio of LFMP/C as the 5% blend, 10% blend, 20% blend, and 30% blend. The whole milling process was carried out in dry conditions with the dry materials and oven-dried milling balls.

The electrode slurry was constituted by 80% active material, 10% polyvinylidene fluoride (battery grade) as a binder, and 10% acetylene black (battery grade) as a conductive agent dispersed in adequate *N*-methyl pyrrolidone (battery grade) solvent at room temperature. An electrode film was obtained by spreading the slurry on an aluminum foil uniformly and drying in a vacuum oven at 80 °C for at least 12 h to remove the redundant solvent and moisture. Then, the dried film was punched into a circular electrode with a diameter of 12 mm and a loading mass of active materials about 2.65 mg/cm^2. The electrochemical properties of NCM523, LFMP/C, and the blend materials were evaluated by a CR2016 type coin cell configuration, which was assembled by sandwiching the polypropylene separator (Celgard 2400) between the blended cathode piece and lithium metal in a glovebox filled with an Ar atmosphere. The electrolyte was 1 M $LiPF_6$ salt dissolved in an ethylene carbonate (EC) and dimethyl carbonate (DMC) (1:1, w/w) solvent.

2.2. Material Characterization. The XRD data were obtained on Rigaku XRD MiniFlex600 with Cu Kα radiation scanning from 10° to 90° at a speed of 2° min^{-1} at a step angle of 0.02° under 40 kV and 15 mA. Field emission scanning electron microscopy (SEM, Hitachi S-4800) was used to characterize the microstructure and micromorphology of NCM523, LFMP/C, and blend materials at an acceleration voltage of 20 kV.

2.3. Electrochemical Measurement. The electrochemical performance of CR2016 cells was tested on Neware BTS type battery testers (Shenzhen, China) at room temperature. The cells were charged with a constant-current (CC) and constant-voltage (CV) mode in the voltage range of 3.0–4.3 V. The cutoff current of CV charge process was set as 1/10 of the CC process. The current value of the tested cell was based on the actual specific capacities of NCM523 (160 mA h/g) and LFMP/C (130 mA h/g).

The rate capacity tests were conducted at 0.2, 0.5, 1, 2, 5, and 0.2 C successively, and each C-rate involved five CC cycles. The theoretical rate performance of the blend material was simulated on COMSOL Multiphysics on the assumptive premise that the two single materials physically mingle without any mutual effects on electrochemical property, based on the actual performance of NCM523 and LFMP/C at 0.2 C. The detailed description can be found in the Supporting Information.

2.4. DSC Characterization. The DSC properties of cathode materials are characterized by a simultaneous thermal analysis (449 F3, Netzsch) with a step temperature of 5 °C/min from 35 to 400 °C. The cells charged to 4.3 V after two CC–CV cycles were disassembled carefully to recover the delithiated cathode piece. Then, the piece was soaked in DMC for 1 h and rinsed with fresh DMC three times to wash off the residual lithium salt and other impurities. The cleaned cathode piece was dried in a glovebox naturally, and then the material was scraped from the electrode piece. Finally, the scraped materials and moderate electrolyte with a ratio of 1 g:1 mL were filled in a hermetic steel crucible together for the DSC test. All steps above were operated in an Ar atmosphere glovebox to ensure isolation from air and moisture.

3. RESULTS AND DISCUSSION

3.1. Structural Characterization. The SEM images of NCM523, LFMP/C, and blend materials are shown in Figure 1, and the size distributions of NCM523 and LFMP/C are shown in Figure S4. NCM523 is composed of a typically globoid secondary structure with an average diameter of 4–5 μm, and LFMP/C is constituted by larger spheres with diameters of 9–10 μm. The particle size distributions of both two individual materials are uniform. It is clear that the low-speed ball-milling

DOI: 10.1021/acsami.8b02102
ACS Appl. Mater. Interfaces 2018, 10, 16458–16466

mingles the blend materials uniformly without destroying the physical structure and morphology of NCM523 and LFMP/C. In addition, the quantity of LFMP/C in the view field of SEM picture increases along with the weight percent increasing.

Figure 2 demonstrates the XRD patterns of NCM523, LFMP/C, and the blend simples. The characteristic peak of

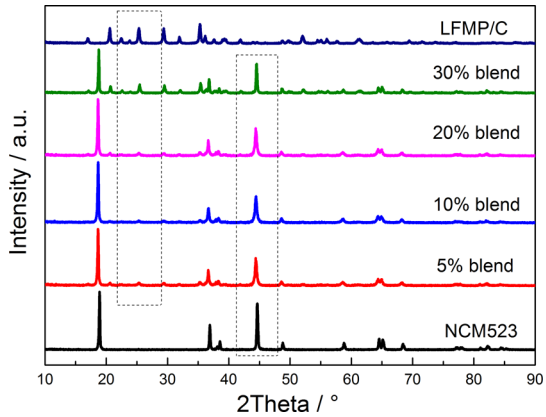

Figure 2. XRD patterns of NCM523, LFMP/C, and the blend materials.

NCM523 can be assigned to the layered α-$NaFeO_2$ ($LiCoO_2$, PDF#77-1370), and the pattern of LFMP/C can be attributed to the orthorhombic olivine structure (LFP, PDF#81-1173). It can be concluded that the ball-milling process does not make any destruction to the crystalline structures of the two individual materials, and all blend materials display the sum characteristic peaks of the two individual materials. The characteristic peak intensity of LFMP/C in the blended materials grows evidently along with the weight percent of LFMP/C increasing from 5 to 30%.

3.2. Electrochemical Properties at Room Temperature. The first charge and discharge curves of NCM523 and LFMP/C are exhibited in Figure 3, consisting of CC−CV (I < C/10) charge and CC discharge steps between 3 and 4.3 V. There are obvious charge−discharge plateaus of LFMP/C at about 3.5−3.6 V and 4.0−4.1 V, corresponding to the redox potential of Fe^{2+}/Fe^{3+} and Mn^{2+}/Mn^{3+}, respectively, whereas the plateaus of NCM523 are in a range of 3.6−4.2 V.

Comparing the cycle performance of all samples in Figure 4, it is concluded that the blend cathodes retain the excellent cycling properties of NCM523 with a compromise discharge specific capacity between NCM523 and LFMP/C. The capacity retention of LFMP/C after 100 cycles at a current of 1 C is poor because of its low electronic conductivity.[27−29] By contrast, both NCM523 and the blend cathodes exhibit a satisfying cycle behavior.

When the LFMP/C ratio in the blend materials is no more than 10%, LFMP/C would make significant contribution to transmission of Li^+ among cathode material particles by enlarging the particles gaps of cathode materials relatively. Moreover, the contiguous points of NCM523 with electrolyte and their parasitic reactions would decrease[30,31] for importing more stable LFMP/C. In contrast, when the weight ratio of LFMP/C is higher than 10%, the inferior conductivity of LFMP/C dominates, leading to a decline of capacity retention after cycling. We have also explored the electrochemical impedance spectroscopy (EIS) curves of NCM523 and blend cathodes, as shown in Figure 4c.

From the profiles of EIS, it can be concluded that the Li^+ diffusion resistances in the solid phase (W_o) of the NCM523, 5% blend, 10% blend, 20% blend, and 30% blend cathodes exhibit the fitting resistances of 24.63, 43.85, 39.26, 58.21, and 88.17 Ω, respectively. This indicates that the 10% blend material has better Li^+ diffusion in the solid phase among all blend materials, proving the conclusion obtained by the cycle performance indirectly.

3.3. Simulative Performance. The parameters of two single cathodes are used in the simulation of the blend system directly, and the details of the simulation process are described in the simulation section of the Supporting Information. The simulated results match well with the experimental discharged curves during the whole procedure at low rates, only a little deviation at high ones, as shown in Figure 5. The correlation coefficients of the experimental and simulated curves at 0.2, 0.5, 1, 2, and 5 C are 0.994429, 0.993279, 0.985756, 0.980421, and 0.979671, respectively. A correlation coefficient close to 1 indicates that the two curves have a good correlation. Similar voltage deviations at high rates can be observed in the previous literature.[32,33] The deviation between experiment and simulation at high C-rates is attributed to the polarization and the intereffects of the two single cathode materials. According to the previous works,[32,34,35] the distribution of Li^+ in the active material affects the electronic conductivity, which further dominates the rate performance of LIBs. However, in our simulation work, the electronic conductivity and diffusion coefficients are all constant values obtained by using the parameters from single NCM523 and LFMP/C at a low C-rate of 0.2 C. When performed at a large current, the distribution of Li^+ and electronic conductivity could not be as same as that at a

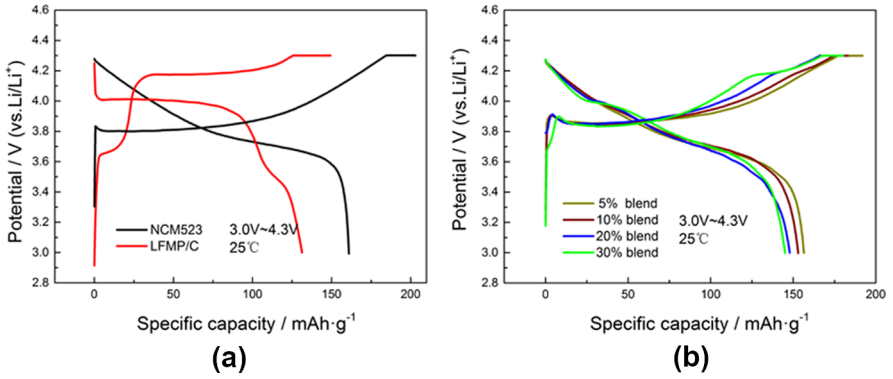

Figure 3. First charge and discharge curves: (a) NCM523 and LFMP/C and (b) the blend cathodes.

DOI: 10.1021/acsami.8b02102
ACS Appl. Mater. Interfaces 2018, 10, 16458−16466

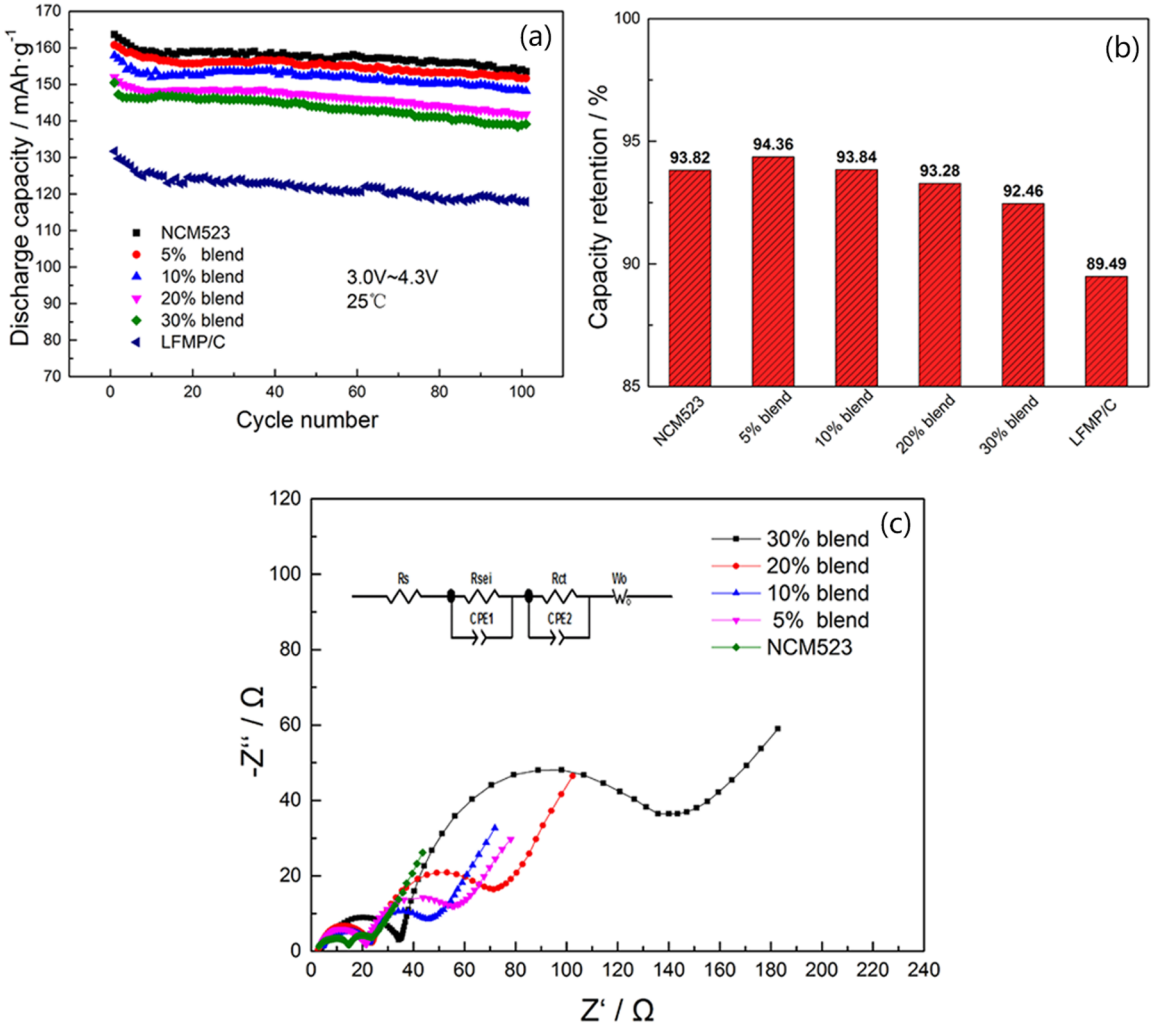

Figure 4. (a) Discharge capacity and (b) capacity retention after 100 cycles of NCM523, LFMP/C, and blend cathodes and (c) EIS curves and equivalent circuit for NCM523 and blend cathodes. R_s: solution resistance; R_{SEI}: solid electrolyte interface (SEI) film resistance; R_{ct}: charge-transfer resistance; and W_o: Li^+ diffusion resistance in the solid phase.

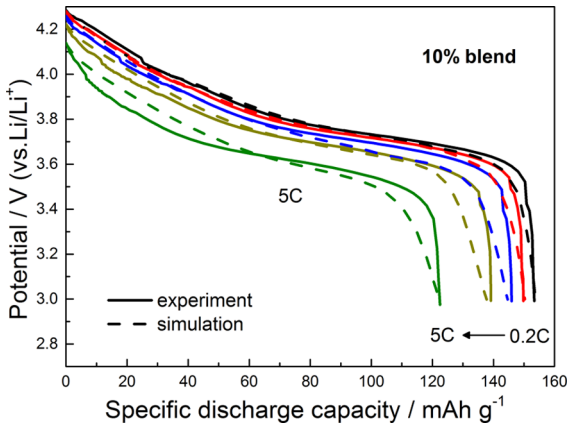

Figure 5. Experimental and simulative rate performance of the 10% blend cathode material. The rate current is 0.2−5 C.

small current, which could lead to an obvious deviation when performed at a high C-rate. In general, the simulation has a favorable conformity with the experiment.

3.4. DSC Analysis. One of the most serious thermal phenomenons in LIBs is the reaction between the electrochemically delithiated cathode and the organic solvent of electrolyte at high temperatures.[31,36−38] For a runaway process in LIBs, the max value of heat flow and total heat released from the cathode and electrolyte system usually play a decisive role. Comparing the max value of heat flow in DSC, it can be found that all values of blend cathodes and electrolyte system do not exceed that of the NCM523, indicating that the addition of LFMP/C in the blend cathode can decrease this value distinctly. However, there is no obvious liner relation between the thermal performance and the weight ratio of LFMP/C in the blend cathode. As shown in Figures 6 and 7, the max heat flow values of NCM523, 5, 10, 20, and 30% blend cathodes are 7.625 mW/mg at 303.44 °C, 3.210 mW/mg at 302.91 °C, 2.478 mW/mg at 303.38 °C, 2.982 mW/mg at 262.63 °C, and 3.517 mW/mg at 256.23 °C, respectively.

The value of max heat flow decreases along with the percent of LFMP/C in the blend cathode when the percent is under 10%, but the value increases when the percent is over 20%. It may be that the exothermic peak at about 303 °C, which belongs to NCM523, declines along with the ratio of NCM523 decreasing accompanied by LFMP/C increasing. At the same time, the increasing LFMP/C induces other side reactions that broaden the exothermic peak at about 260 °C.

DOI: 10.1021/acsami.8b02102
ACS Appl. Mater. Interfaces 2018, 10, 16458−16466

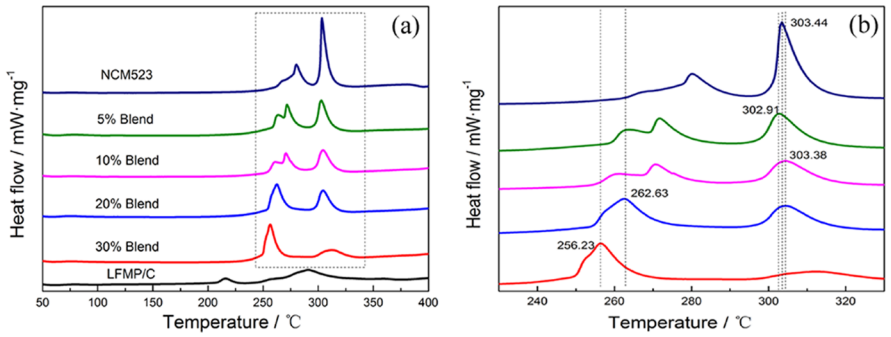

Figure 6. (a) DSC curves of NCM523, LFMP/C, and the blend materials and (b) enlarged details of NCM523 and the blend materials.

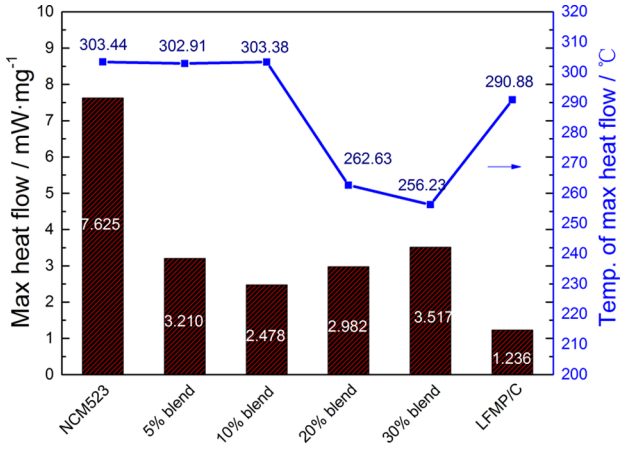

Figure 7. Max heat flow and corresponding temperature of NCM523, LFMP/C, and the blend materials.

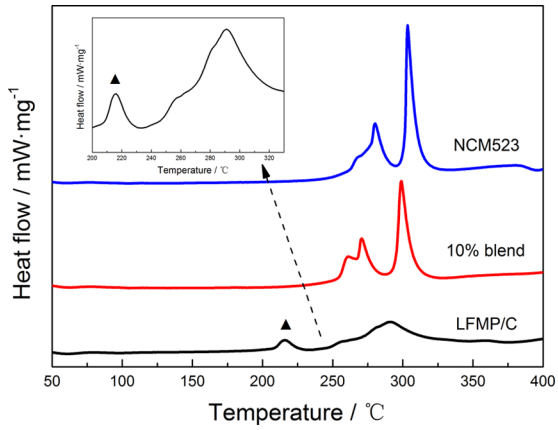

Figure 8. Exothermic peak comparison of three DSC curves.

It can be observed from the DSC curves that the onset temperature of LFMP/C and electrolyte system is about at 207 °C, lower than those of NCM523 and blend cathodes. Nevertheless, the max value of heat flow is only 1.236 mW/mg, and the total heat released during the whole exothermic process is 472.8 J/g, much lower than those of NCM523 and the blend cathode as well. It means that thermal reaction of the LFMP/C system is extremely gentle and has little possibility of resulting in a severe runaway, even though batteries are abused. In consideration of both electrochemical and thermal properties, 10% LFMP/C in the blend cathode materials is selected as the most adaptable weight ratio.

The 10% blend material shows onset and peak temperatures similar to those of NCM523, with a much lower value of maximum heat flow and total heat quantity, which means that the blend cathode will release pretty less heat instantaneously as reacting with electrolyte than the NCM523 system. This effect decreases the possibility of thermal runaway caused by delithiated cathode with electrolyte, which further proves that the blend cathode material has more extraordinary thermostability than the single NCM cathode.

Comparing the DSC curves in Figure 8 and the data of blend cathode with those of the two single cathodes in Table 1, we concluded that the blend is beyond just blend. The total heat release of the blend cathode is less than direct calculated values from the two single cathodes by weighing according to their mass fraction. Also, the exothermic peak at around 207 °C from LFMP/C disappears in the blend system as well.

There may be a synergistic effect between NCM523 and LFMP/C. LFMP/C in the blend cathode retards the whole thermal procedure, and the existence of NCM523 eliminates the exothermic peak started at 207 °C of LFMP/C.

In order to confirm the reason that the exothermic peak at 207 °C appears, the thermal performances of EC/DMC, electrolyte, and delithiated LFMP/C with an electrolyte system are studied by the DSC tests in Figure 9. It is obvious that EC/DMC remains stable until heating up to 310 °C without any exothermic phenomenon. As $LiPF_6$ is added into EC/DMC, a distinct exothermic peak appears at about 260 °C. Hence, the exothermic peak at 207 °C is attributed to the addition of LFMP/C in the delithiated LFMP/C with an electrolyte system.

$LiPF_6$ tends to react with the trace H_2O in the electrolyte to form HF, followed by a self-decomposition at high temperatures to form LiF and PF_5.[39−41] The existence of HF and Lewis acid PF_5 will result in the decomposition of organic solvent EC and DMC along with releasing heat. It is proposed that the exothermic peak at 207 °C in the delithiated LFMP/C−electrolyte system is related to the trace H_2O and HF formed by the reaction between trace H_2O and $LiPF_6$.

To demonstrate the above assumption, the moderate *N*,*N*-diethylamino trimethylsilane (DEATMS, Aladdin, 98%) is added into the electrolyte system. According to previous research studies,[42] DEATMS can serve as an excellent additive in an electrolyte for eliminating H_2O and HF in order to improve the electrochemical stability of LIBs. Figure 10 shows the DSC curves of the delithiated LFMP/C−electrolyte system and the delithiated LFMP/C−electrolyte with a DEATMS system. Obviously, the first exothermic peak at about 207 °C in the delithiated LFMP/C−electrolyte system disappears because of the existence of DEATMS. This proof further verifies that

DOI: 10.1021/acsami.8b02102
ACS Appl. Mater. Interfaces 2018, 10, 16458−16466

Table 1. DSC Data of NCM523, LFMP/C, and Blend Material

	onset temperature (°C)	peak temperature (°C)	maximal heat flow (mW/mg)	total heat (J/g)	calculated heat (J/g)	reduction of heat (J/g)
NCM523	258.40	303.44	7.625	967.7		
10% blend	251.69	303.38	2.478	829.7	918.2	88.5
LFMP/C	207.01	290.88	1.236	472.8		

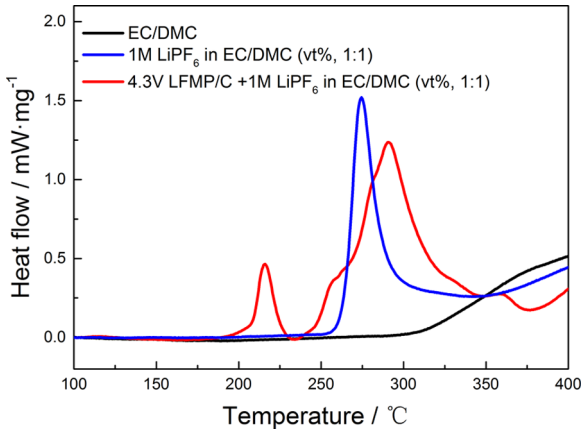

Figure 9. DSC curves of EC/DMC, electrolyte, and delithiated LFMP/C with electrolyte.

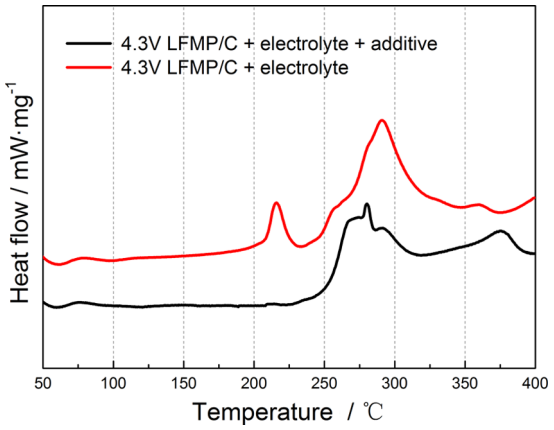

Figure 10. DSC curves of delithiated LFMP/C with an electrolyte system and delithiated LFMP/C with an electrolyte and additive system.

the exothermic peak at 207 °C is resulted from the trace H_2O and HF in the electrolyte.

The further mechanism for the elimination of trace H_2O and HF in our blend cathode is that there may be an interchange of Li^+ and H^+ between NCM and HF without the generation of H_2O, resulting in the disappearance of the exothermic peak at 207 °C.[21,43]

The first exothermic process of delithiated LFMP/C−electrolyte system is finished at about 230 °C, as shown in Figure 8, but there is not any exothermic peak appearing before 250 °C in the blended system. Therefore, 230 °C is selected as the demarcation point for the next exploration about the changes that the delithiated LFMP/C undergoes at high temperatures. The delithiated LFMP/C at room temperature (LFMP/C-RT), the delithiated LFMP/C heated to 230 °C (LFMP/C-230 °C), and the delithiated LFMP/C with an electrolyte system heated to 230 °C (LFMP/C−electrolyte-230 °C) are tested by XRD. All of those samples gained at 230 °C are the products in a sealed DSC process, and then they are recovered in a glovebox filled with Ar and are encapsulated with polyimide tape on a glass slide. Any contact between samples and air is prohibited during the whole course.

The XRD patterns reveal clear differences in the position and intensity among the three samples, shown in Figure 11. As for the crystal structure, LFMP/C-RT is identical to the (Fe,Mn)-PO_4 (PDF#00-037-0478), LFMP/C-230 °C is the same as $(Fe,Mn)_3(PO_4)_2$ (PDF#00-018-0642), and LFMP/C−electrolyte-230 °C is identical to $Mn_2P_2O_7$ (PDF#00-003-0555), which proves that the delithiated LFMP/C has tremendous phase changes because of the generation of HF and trace H_2O at high temperatures.

The same tests are conducted for the blend samples, and the XRD patterns of the blend sample at room temperature, 230 °C, and 230 °C with an electrolyte are shown in Figure 12. Almost all of them retain the same peak position and intensity, and there is no new phase generated, although at high temperatures and with an electrolyte. Compared with the XRD results in Figure 11, it can be concluded that NCM523 served as the component to stabilize the structure of delithiated LFMP/C with an electrolyte at high temperatures. It is also in accordance with the exothermic phenomenon of the blend materials that there is not any reaction between the blend material and the electrolyte until 230 °C, as shown in Figure 8.

3.5. Electrochemical Properties at 55 °C. The electrochemical properties of NCM523, LFMP/C, and 10% blend material at 55 °C and 1 C are exhibited in Figure 13. It can be observed from Figure 13a that the specific capacities of NCM523, LFMP/C, and 10% blend material are 181.29, 139.24, and 174.19 mA h/g, respectively. Comparing the cycle performance at 55 °C and that at 25 °C (Figure 3), it is obvious that all cathode materials show a higher specific capacity at 55 °C than at 25 °C. It is mainly because that the kinetic performance is enhanced at higher temperatures. However, the capacity retention of LFMP/C decreases severely after long cycles than room temperature (Figure 13b). The unfavorable performance is attributed to more HF coming from the electrolyte at high temperatures, which attracts LFMP/C and leads to the dissolution of Mn during the cycling process.[44,45] By contrast, the 10% blend displays a better cycling performance at 55 °C than individual LFMP/C in Figure 13b, which is ascribed to the synergistic effects between NCM523 and LFMP/C described in DSC analysis.

4. CONCLUSIONS

The NCM523−LFMP/C blend cathode materials are prepared by a simple mechanical ball-milling method without any destruction of the physical structure and crystal structure. The blend materials with 10% LFMP/C exhibit better capacity retention after 100 cycles than the single LFMP/C and other LFMP/C weight ratio of the blend materials. The electrochemical property of the blend cathode materials prepared by a simple mechanical method is predictable by theoretical methods using the COMSOL Multiphysics. All blend cathode materials present better thermal stability than single NCM523, whereas 10% LFMP/C in the blend cathode materials is the

DOI: 10.1021/acsami.8b02102
ACS Appl. Mater. Interfaces 2018, 10, 16458−16466

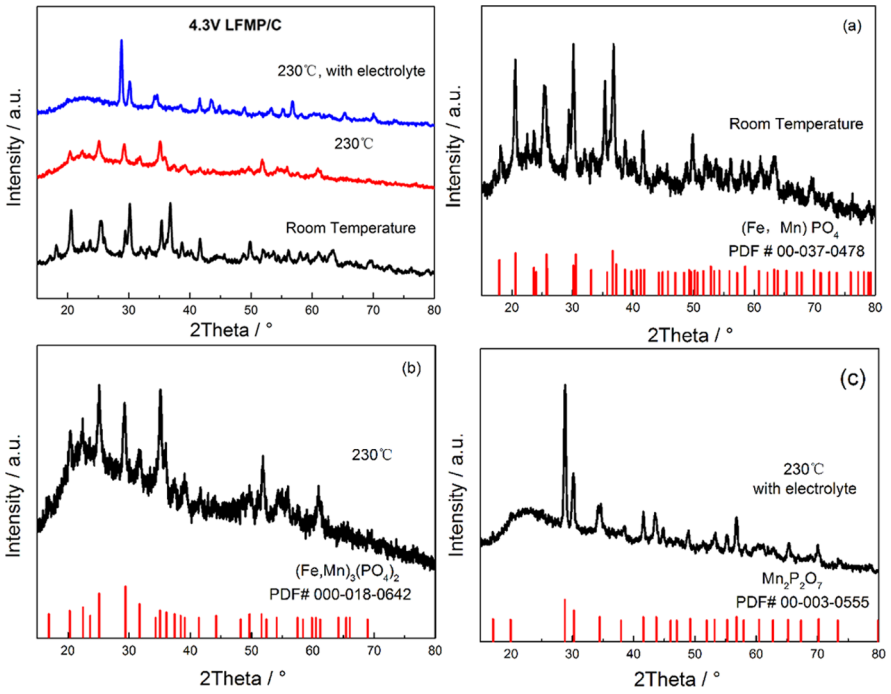

Figure 11. XRD plots of delithiated LFMP/C at (a) room temperature, (b) 230 °C, and (c) 230 °C with an electrolyte.

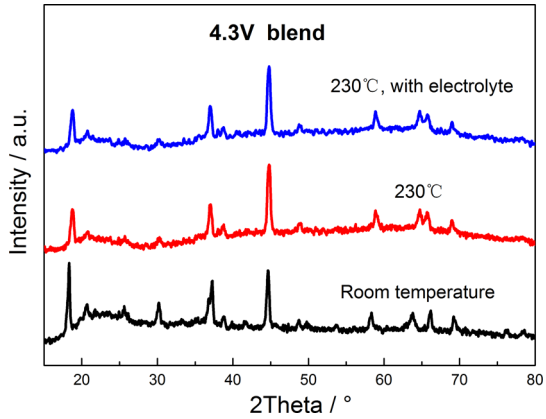

Figure 12. XRD plots of delithiated blend cathode at room temperature, 230 °C, and 230 °C with an electrolyte.

most adaptable as considering both electrochemical and thermal properties simultaneously. The synergistic effects between NCM523 and LFMP/C improve the thermal stability of the blend cathode materials. LFMP/C serves as a component that decreases the total heat release of the delithiated blend cathode, and NCM523 plays a role in eliminating the onset temperature of blend cathode materials by exchanging Li^+ with H^+ to prevent the HF reaction with LFMP/C and electrolyte at high temperatures. We believe that the blend cathode materials combining the advantages of the two single materials, LFMP/C and NCM523, can serve as promising cathodes for lithium ion batteries.

■ ASSOCIATED CONTENT

Supporting Information

The Supporting Information is available free of charge on the ACS Publications website at DOI: 10.1021/acsami.8b02102.

Equilibrium potential, dynamic diffusion coefficient, experimental discharge profile and simulated discharge profile, and particle size of NCM523 and LFMP/C (PDF)

■ AUTHOR INFORMATION

Corresponding Authors

*E-mail: wangjing2015@xmu.edu.cn (J.W.).

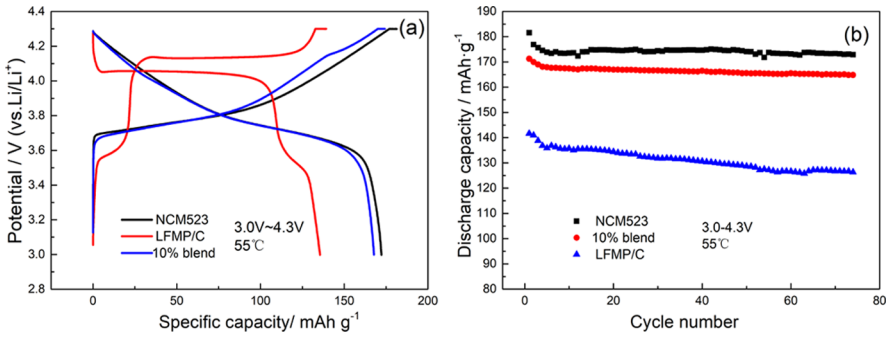

Figure 13. (a) First charge and discharge curves and (b) discharge capacity after 75 cycles.

DOI: 10.1021/acsami.8b02102
ACS Appl. Mater. Interfaces 2018, 10, 16458−16466

*E-mail: jbzhao@xmu.edu.cn (J.Z.).

ORCID

Jinbao Zhao: 0000-0002-2753-7508

Notes

The authors declare no competing financial interest.

■ ACKNOWLEDGMENTS

This work was financially supported by National Key Research and Development Program of China (no. 2017YFB0102000) and National Natural Science Foundation of China (no. 21621091). The authors also wish to express their gratitude to Prof. Daiwei Liao for his valuable suggestions.

■ REFERENCES

(1) Roy, P.; Srivastava, S. K. Nanostructured Anode Materials for Lithium Ion Batteries. *J. Mater. Chem. A* **2015**, *3*, 2454−2484.

(2) Tarascon, J.-M.; Armand, M. Issues and Challenges Facing Rechargeable Lithium Batteries. *Nature* **2001**, *414*, 359−367.

(3) Lu, L.; Han, X.; Li, J.; Hua, J.; Ouyang, M. A Review on the Key Issues for Lithium-Ion Battery Management in Electric Vehicles. *J. Power Sources* **2013**, *226*, 272−288.

(4) Zhang, S. S. A Review on Electrolyte Additives for Lithium-Ion Batteries. *J. Power Sources* **2006**, *162*, 1379−1394.

(5) Hannan, M. A.; Lipu, M. S. H.; Hussain, A.; Mohamed, A. A Review of Lithium-Ion Battery State of Charge Estimation and Management System in Electric Vehicle Applications: Challenges and Recommendations. *Renewable Sustainable Energy Rev.* **2017**, *78*, 834−854.

(6) Feng, X.; Ouyang, M.; Liu, X.; Lu, L.; Xia, Y.; He, X. Thermal Runaway Mechanism of Lithium Ion Battery for Electric Vehicles: A Review. *Energy Storage Mater.* **2018**, *10*, 246−267.

(7) Bandhauer, T. M.; Garimella, S.; Fuller, T. F. A Critical Review of Thermal Issues in Lithium-Ion Batteries. *J. Electrochem. Soc.* **2011**, *158*, R1.

(8) Zhang, W.-J. A Review of the Electrochemical Performance of Alloy Anodes for Lithium-Ion Batteries. *J. Power Sources* **2011**, *196*, 13−24.

(9) Zhang, Y.; Mo, G.; Li, X.; Zhang, W.; Zhang, J.; Ye, J.; Huang, X.; Yu, C. A Graphene Modified Anode to Improve the Performance of Microbial Fuel Cells. *J. Power Sources* **2011**, *196*, 5402−5407.

(10) Zuo, X.; Zhu, J.; Müller-Buschbaum, P.; Cheng, Y.-J. Silicon Based Lithium-Ion Battery Anodes: A Chronicle Perspective Review. *Nano Energy* **2017**, *31*, 113−143.

(11) Liu, Z.; Yu, A.; Lee, J. Y. Synthesis and Characterization of LiNi1− x − yCoxMnyO2 as the Cathode Materials of Secondary Lithium Batteries. *J. Power Sources* **1999**, *81*−*82*, 416−419.

(12) Schipper, F.; Erickson, E. M.; Erk, C.; Shin, J.-Y.; Chesneau, F. F.; Aurbach, D. Review—Recent Advances and Remaining Challenges for Lithium Ion Battery Cathodes: I. Nickel-Rich, LiNixCoyMnzO2. *J. Electrochem. Soc.* **2017**, *164*, A6220−A6228.

(13) Zhu, W.; Liu, D.; Trottier, J.; Gagnon, C.; Guerfi, A.; Julien, C. M.; Mauger, A.; Zaghib, K. Comparative Studies of the Phase Evolution in M-Doped LixMn1.5Ni0.5O4 (M=Co, Al, Cu and Mg) by In-Situ X-ray Diffraction. *J. Power Sources* **2014**, *264*, 290−298.

(14) Akita, T.; Tabuchi, M.; Nabeshima, Y.; Tatsumi, K.; Kohyama, M. Electron Microscopy Analysis of Ti-Substituted Li2MnO3 Positive Electrode before and after Carbothermal Reduction. *J. Power Sources* **2014**, *254*, 39−47.

(15) Aurbach, D.; Srur-Lavi, O.; Ghanty, C.; Dixit, M.; Haik, O.; Talianker, M.; Grinblat, Y.; Leifer, N.; Lavi, R.; Major, D. T. Studies of Aluminum-Doped LiNi0.5Co0.2Mn0.3O2: Electrochemical Behavior, Aging, Structural Transformations, and Thermal Characteristics. *J. Electrochem. Soc.* **2015**, *162*, A1014−A1027.

(16) Wu, Z.; Ji, S.; Liu, T.; Duan, Y.; Xiao, S.; Lin, Y.; Xu, K.; Pan, K. Aligned Li+ Tunnels in Core-shell Li(NixMnyCoz)O2@LiFePO4 Enhances Its High Voltage Cycling Stability as Li-Ion Battery Cathode. *Nano Lett.* **2016**, *16*, 6357−6363.

(17) Duan, J.; Wu, C.; Cao, Y.; Du, K.; Peng, Z.; Hu, G. Enhanced Electrochemical Performance and Thermal Stability of LiNi0.80-Co0.15Al0.05O2 via Nano-Sized LiMnPO4 Coating. *Electrochim. Acta* **2016**, *221*, 14−22.

(18) Cho, W.; Kim, S.-M.; Song, J. H.; Yim, T.; Woo, S.-G.; Lee, K.-W.; Kim, J.-S.; Kim, Y.-J. Improved Electrochemical and Thermal Properties of Nickel Rich LiNi0.6Co0.2Mn0.2O2 Cathode Materials by SiO2 Coating. *J. Power Sources* **2015**, *282*, 45−50.

(19) Lee, K.-S.; Myung, S.-T.; Kim, D.-W.; Sun, Y.-K. AlF 3 -Coated LiCoO2 and Li[Ni1/3Co1/3Mn 1/3]O2 Blend Composite Cathode for Lithium Ion Batteries. *J. Power Sources* **2011**, *196*, 6974−6977.

(20) Tran, H. y.; Täubert, C.; Fleischhammer, M.; Axmann, P.; Küppers, L.; Wohlfahrt-Mehrens, M. LiMn2O4 Spinel/LiNi0.8-Co0.15Al0.05O2 Blends as Cathode Materials for Lithium-Ion Batteries. *J. Electrochem. Soc.* **2000**, *158*, A556.

(21) Wang, J.; Yu, Y.; Li, B.; Zhang, P.; Huang, J.; Wang, F.; Zhao, S.; Gan, C.; Zhao, J. Thermal Synergy Effect between LiNi0.5Co0.2Mn0.3O2 and LiMn2O4 Enhances the Safety of Blended Cathode for Lithium Ion Batteries. *ACS Appl. Mater. Interfaces* **2016**, *8*, 20147−20156.

(22) Xiao, P. F.; Ding, B.; Lai, M. O.; Lu, L. High Performance LiMn1-xFexPO4 ($0 \leq x \leq 1$) Synthesized via a Facile Polymer-Assisted Mechanical Activation. *J. Electrochem. Soc.* **2013**, *160*, A918−A926.

(23) Meligrana, G.; Lupo, F. D.; Ferrari, S.; Destro, M.; Bodoardo, S.; Garino, N.; Gerbaldi, C. Surfactant-Assisted Mild Hydrothermal Synthesis to Nanostructured Mixed Orthophosphates LiMnyFe1−yPO4/C Lithium Insertion Cathode Materials. *Electrochim. Acta* **2013**, *105*, 99−109.

(24) Kim, J.; Park, K.-Y.; Park, I.; Yoo, J.-K.; Hong, J.; Kang, K. Thermal Stability of Fe−Mn Binary Olivine Cathodes for Li Rechargeable Batteries. *J. Mater. Chem.* **2012**, *22*, 11964.

(25) Noh, H.-J.; Youn, S.; Yoon, C. S.; Sun, Y.-K. Comparison of the Structural and Electrochemical Properties of Layered Li[NixCoyMnz]-O2 (x = 1/3, 0.5, 0.6, 0.7, 0.8 and 0.85) Cathode Material for Lithium-Ion Batteries. *J. Power Sources* **2013**, *233*, 121−130.

(26) Bak, S.-M.; Hu, E.; Zhou, Y.; Yu, X.; Senanayake, S. D.; Cho, S.-J.; Kim, K.-B.; Chung, K. Y.; Yang, X.-Q.; Nam, K.-W. Structural Changes and Thermal Stability of Charged LiNixMnyCozO2 Cathode Materials Studied by Combined In Situ Time-Resolved XRD and Mass Spectroscopy. *ACS Appl. Mater. Interfaces* **2014**, *6*, 22594−22601.

(27) Molenda, J.; Ojczyk, W.; Świerczek, K.; Zając, W.; Krok, F.; Dygas, J.; Liu, R. Diffusional Mechanism of Deintercalation in LiFe1-yMnyPO4 Cathode Material. *Solid State Ionics* **2006**, *177*, 2617−2624.

(28) Muraliganth, T.; Manthiram, A. Understanding the Shifts in the Redox Potentials of Olivine LiM1−yMyPO4 (M = Fe, Mn, Co, and Mg) Solid Solution Cathodes. *J. Phys. Chem. C* **2010**, *114*, 15530−15540.

(29) Martha, S. K.; Grinblat, J.; Haik, O.; Zinigrad, E.; Drezen, T.; Miners, J. H.; Exnar, I.; Kay, A.; Markovsky, B.; Aurbach, D. LiMn0.8Fe0.2PO4 : An Advanced Cathode Material for Rechargeable Lithium Batteries. *Angew. Chem., Int. Ed.* **2009**, *48*, 8559−8563.

(30) Li, J.; Downie, L. E.; Ma, L.; Qiu, W.; Dahn, J. R. Study of the Failure Mechanisms of LiNi0.8Mn0.1Co0.1O2 Cathode Material for Lithium Ion Batteries. *J. Electrochem. Soc.* **2015**, *162*, A1401−A1408.

(31) Smith, A. J.; Burns, J. C.; Xiong, D.; Dahn, J. R. Interpreting High Precision Coulometry Results on Li-ion Cells. *J. Electrochem. Soc.* **2011**, *158*, A1136.

(32) Appiah, W. A.; Park, J.; van Khue, L.; Lee, Y.; Choi, J.; Ryou, M.-H.; Lee, Y. M. Comparative Study on Experiments and Simulation of Blended Cathode Active Materials for Lithium Ion Batteries. *Electrochim. Acta* **2016**, *187*, 422−432.

(33) Rashid, M.; Gupta, A. Experimental Assessment and Model Development of Cycling Behavior in Li-Ion Coin Cells. *Electrochim. Acta* **2017**, *231*, 171−184.

(34) Nobili, F.; Dsoke, S.; Minicucci, M.; Croce, F.; Marassi, R. Correlation of AC-Impedance and In Situ X-ray Spectra of LiCoO2. *J. Phys. Chem. B* **2006**, *110*, 11310−11313.

DOI: 10.1021/acsami.8b02102
ACS Appl. Mater. Interfaces 2018, 10, 16458−16466

(35) Arora, P.; Doyle, M.; Gozdz, A. S.; White, R. E.; Newman, J. Comparison between Computer Simulations and Experimental Data for High-Rate Discharges of Plastic Lithium-Ion Batteries. *J. Power Sources* **2000**, *88*, 219−231.
(36) Röder, P.; Stiaszny, B.; Ziegler, J. C.; Baba, N.; Lagaly, P.; Wiemhöfer, H.-D. The Impact of Calendar Aging on the Thermal Stability of a LiMn2O4−Li(Ni1/3Mn1/3Co1/3)O2/Graphite Lithium-Ion Cell. *J. Power Sources* **2014**, *268*, 315−325.
(37) Röder, P.; Baba, N.; Wiemhöfer, H.-D. A Detailed Thermal Study of a Li[Ni0.33Co0.33Mn0.33]O2/LiMn2O4-Based Lithium Ion Cell by Accelerating Rate and Differential Scanning Calorimetry. *J. Power Sources* **2014**, *248*, 978−987.
(38) Escobar-Hernandez, H. U.; Gustafson, R. M.; Papadaki, M. I.; Sachdeva, S.; Mannan, M. S. Thermal Runaway in Lithium-Ion Batteries: Incidents, Kinetics of the Runaway and Assessment of Factors Affecting Its Initiation. *J. Electrochem. Soc.* **2016**, *163*, A2691−A2701.
(39) Martha, S. K.; Haik, O.; Zinigrad, E.; Exnar, I.; Drezen, T.; Miners, J. H.; Aurbach, D. On the Thermal Stability of Olivine Cathode Materials for Lithium-Ion Batteries. *J. Electrochem. Soc.* **2011**, *158*, A1115.
(40) Yamada, A.; Kudo, Y.; Liu, K.-Y. Reaction Mechanism of the Olivine-Type Lix(Mn0.6Fe 0.4)PO4 (0≤x≤1). *J. Electrochem. Soc.* **2001**, *148*, A747.
(41) Chen, G.; Richardson, T. J. Thermal Instability of Olivine-Type LiMnPO4 Cathodes. *J. Power Sources* **2010**, *195*, 1221−1224.
(42) Haregewoin, A. M.; Wotango, A. S.; Hwang, B.-J. Electrolyte Additives for Lithium Ion Battery Electrodes: Progress and Perspectives. *Energy Environ. Sci.* **2016**, *9*, 1955−1988.
(43) Numata, T.; Amemiya, C.; Kumeuchi, T.; Shirakata, M.; Yonezawa, M. Advantages of Blending LiNi0.8Co0.2O2 into Li1+xMn2− xO4 Cathodes. *J. Power Sources* **2001**, *97*, 358−360.
(44) Oh, S.-M.; Myung, S.-T.; Choi, Y. S.; Oh, K. H.; Sun, Y.-K. Co-Precipitation Synthesis of Micro-Sized Spherical LiMn0.5Fe0.5PO4 Cathode Material for Lithium Batteries. *J. Mater. Chem.* **2011**, *21*, 19368.
(45) Oh, S.-M.; Myung, S.-T.; Park, J. B.; Scrosati, B.; Amine, K.; Sun, Y.-K. Double-Structured LiMn0.85Fe0.15PO4 Coordinated with LiFePO4 for Rechargeable Lithium Batteries. *Angew. Chem.* **2012**, *124*, 1889−1892.

DOI: 10.1021/acsami.8b02102
ACS Appl. Mater. Interfaces 2018, 10, 16458−16466